

Article

# Finite-Time Attitude Control of Quadrotor Unmanned Aerial Vehicle with Disturbance and Actuator Saturation

Zheng Zhang, Xingwei Li \* and Lilian Zhang

College of Intelligence Science and Technology, National University of Defense Technology, Changsha 410073, China; zhangzheng0624@nudt.edu.cn (Z.Z.); lilianzhang@nudt.edu.cn (L.Z.)

\* Correspondence: lxw\_mmoml@nudt.edu.cn; Tel.: +86-1357-4830-557

**Featured Application:** This work addresses issues related to unknown disturbances and actuator saturation during quadrotor UAV flight.

**Abstract:** This paper introduces a nonlinear dynamic inversion control algorithm designed to address unknown disturbances and actuator saturation issues in unmanned aerial vehicle (UAV) attitude control. The algorithm is based on a combination of finite-time disturbance observer and anti-saturation auxiliary system, which ensures the rapid convergence of attitude tracking error. Firstly, based on the Newton–Euler equations, this paper establishes a model of the attitude system for quadrotor UAVs, and this paper eliminates the small-angle flight assumption. Secondly, considering the actuator saturation problem, an anti-saturation auxiliary control system is designed to shorten the time when the control volume is in the saturation interval and achieve finite-time convergence of the attitude error. And then, to improve the robustness of the controller, this paper proposes a disturbance observer based on the finite-time stability theory, which achieves a continuous smooth output of the observation results by introducing a hyperbolic tangent function in the observer, so that the observation error can be converged to zero in a finite time. Finally, it is demonstrated by Simulink simulation that the attitude error and the observation error converge quickly to zero.

**Keywords:** finite-time control; attitude control; finite-time disturbance observer; actuator saturation; anti-saturation



**Citation:** Zhang, Z.; Li, X.; Zhang, L. Finite-Time Attitude Control of Quadrotor Unmanned Aerial Vehicle with Disturbance and Actuator Saturation. *Appl. Sci.* **2024**, *14*, 3639. <https://doi.org/10.3390/app14093639>

Academic Editor: Jérôme Morio

Received: 25 March 2024

Revised: 14 April 2024

Accepted: 21 April 2024

Published: 25 April 2024



**Copyright:** © 2024 by the authors. Licensee MDPI, Basel, Switzerland. This article is an open access article distributed under the terms and conditions of the Creative Commons Attribution (CC BY) license (<https://creativecommons.org/licenses/by/4.0/>).

## 1. Introduction

Nowadays, quadrotor UAVs have become an important tool and a technology carrier in various fields. Because of its advantages such as good mobility and easy operation, it is gradually becoming an indispensable technological tool in various fields of modern society, bringing new possibilities and opportunities for the development and progress of human beings [1–3]. However, the control problem of quadrotor UAV has been a popular research direction in the control discipline because of its strong nonlinearity, strong coupling, underactuation, and multiple inputs and multiple outputs.

The ultimate control goal of a quadrotor UAV is to achieve precise position control, while good attitude control is a prerequisite for precise position control. In the past decades, many studies have studied the attitude control problem. The control methods can be divided into linear control methods and nonlinear control methods. The common linear control methods are PID and LQR. As early as 2005, Altug et al. [4] used a PID algorithm to implement attitude control on a small quadrotor aircraft and achieved good control results. However, the PID algorithm also has some problems, such as parameter tuning relying on the designer's experience, sensitivity to noise, limitation to linear systems, and lack of stability proof. To address these problems, Lin et al. [5] combined the PID and the backstepping method to give a tuning range of PID parameters. For the problems of slow tuning process and large overshoot, Xu et al. [6] proposed an adaptive control method based on single neuron PID, which can enhance the robustness of the controller

by adaptively adjusting parameters. Kazim et al. [7] use a particle swarm algorithm to optimize the proportional and differential parameters in the position controller. They also designed a robust adaptive integral backstepping-based attitude controller to achieve the stable control of the UAV under external wind disturbances. Elias et al. [8] proposed an LQR control method based on gain scheduling, and this control method can select different feedback gain matrices according to the error of the system.

Although the above linear control methods can achieve good attitude control, they are often designed based on a linearized model with small angle assumptions, and when the attitude of the quadrotor UAV changes significantly, the linear control methods often fail to obtain good control results. Therefore, many researchers began to turn their attention to the study of nonlinear control methods [9–13]. Nonlinear dynamic inversion (NDI) [14] is one of the commonly used control algorithms for aircrafts. It is a nonlinear control method based on feedback linearization, which cancels out the nonlinear terms in the original system through the form of state feedback to achieve the linearization of the nonlinear system. Alonge et al. [15] used an approach based on feedback linearization and that utilized extended state observers for the online estimation of unknown disturbances. However, this method requires a high-accuracy system model. Studies [16–18] incorporate an adaptive approach to improve the robustness of NDI. Qiao et al. [19] improved the detrimental effect of the dynamic inversion nonlinear term on error elimination by adding additional feedback to the state feedback link of the dynamic inversion.

Due to the existence of disturbance and modeling errors, methods based on disturbance estimation have received extensive attention from scholars. In the studies [20–23], all of them use the extended state observer (ESO) to estimate the total disturbance in the UAV's attitude system to achieve active disturbance rejection control (ADRC). Based on a dual closed-loop active disturbance suppression generalized predictive control, Cheng et al. [24] proposed a robust controller for quadrature trajectory tracking control. However, in all of the above methods, the observation error converges to zero in an asymptotically convergent manner, which only guarantees the convergence of the observation error at infinite time. With the further development of stabilization control theory, the theory of "finite time control" has gradually emerged. Ríos et al. [25] designed a finite-time sliding mode observer to estimate the disturbance. Inspired by the multivariate super-twisting algorithm, Jiang et al. [26] designed a finite-time disturbance observer (FDO) to estimate the system disturbance, which improves the robustness of the controller. Zhu et al. [27] also took actuator faults as disturbance into account and proposed an FDO to achieve an accurate estimation of disturbance and actuator faults. In the above studies, the output of the observer is prone to a chattering phenomenon due to the presence of sign function terms in the observer. To address this problem, studies [28–31] investigated an FDO based on the homogeneous theory. Lan et al. [31] designed a continuous FDO based on the homogeneous theory and the saturation function method to estimate the disturbance, but when the sampling time becomes longer, this FDO could not achieve a stable output of the observed signals.

In addition, the saturation constraint of the actuator is also a non-negligible problem. In practical systems, the output signal of the actuator frequently experiences amplitude saturation, leading to a situation where the controller struggles to promptly regulate the system state. Concerning the saturation issue, anti-saturation control methods are increasingly categorized into two main groups: active anti-saturation methods [32–35] and passive anti-saturation methods [36–39]. Farid et al. [36] proposed a nonlinear controller based on nested saturation for the rotational speed saturation problem of the quadrotor UAV. Based on this, Li et al. [37] considered a more complex quadrotor UAV model, and the anti-saturation auxiliary system prevents the saturation phenomenon by adaptively adjusting the system error. Different from the study [33], Liu et al. [38] introduced the output of the anti-saturation auxiliary system into the control volume, which also achieved effective control. Sun et al. [39] designed an anti-saturation auxiliary system with non-singularity for the saturation problem in spacecraft attitude control, which achieved the fast

convergence of the auxiliary system state. However, there are fewer studies on finite-time anti-saturation control.

Inspired by the above work, a finite-time disturbance observer and an anti-saturation auxiliary control method (FDOACM) are proposed in this paper with the following main contributions:

- The assumptions based on small-angle flight are eliminated, so that the rate of change of the Euler angle and the angular velocity of the airframe satisfy the nonlinear relationship in an actual flight, and the total disturbance of the system and the actuator saturation are taken into account. The established model better reflects real flight conditions.
- For the saturation problem of the actuator, an anti-saturation auxiliary control system is designed. In the presence of saturation, this anti-saturation auxiliary control system promptly guides the controller’s output moment out of the saturation range by correcting attitude feedback errors. This ensures finite-time convergence of attitude errors in anti-saturation scenarios.
- Targeting the overall disturbance experienced during flight, a disturbance observer rooted in finite-time stability theory is crafted to precisely estimate disturbances. IN contrast with the existing literature-based observers [31,40], the observer proposed in this study not only achieves finite-time convergence of observation errors but also guarantees the continuity of observer output results.

The structure of this paper unfolds as follows: In Section 2, we begin by presenting key lemmas and definitions utilized throughout this work, followed by the establishment of a model depicting a quadrotor UAV attitude system under external disturbances and actuator constraints. Section 3 delineates the algorithm’s design process proposed herein and provides proof regarding the controller’s stability. Section 4 offers simulation results based on the algorithm proposed in this paper. Finally, Section 5 encapsulates the conclusions drawn from this study.

### 2. Preliminaries and Problem Formulation

**Lemma 1.** For  $\forall g_i \in R, i = 1, 2, \dots, n$ , two positive real numbers  $0 < v_1 \leq 1$  and  $v_2 > 1$ , the inequalities that hold are as follows [41]:

$$\left(\sum_{i=1}^n |g_i|\right)^{v_1} \leq \sum_{i=1}^n |g_i|^{v_1} \leq n^{1-v_1} \left(\sum_{i=1}^n |g_i|\right)^{v_1} \tag{1}$$

$$\sum_{i=1}^n |g_i|^{v_2} \leq \left(\sum_{i=1}^n |g_i|\right)^{v_2} \leq n^{v_2-1} \sum_{i=1}^n |g_i|^{v_2} \tag{2}$$

**Lemma 2.** For  $\forall (a, b) \in R^2$ , one can obtain the following [42]:

$$ab \leq \frac{\xi^{\tilde{p}}}{\tilde{p}} |a|^{\tilde{p}} + \frac{1}{\tilde{q}\xi^{\tilde{q}}} |b|^{\tilde{q}} \tag{3}$$

where  $\xi > 0, \tilde{q} > 1, \tilde{p} > 1$ , and  $(\tilde{p} - 1)(\tilde{q} - 1) = 1$ .

**Lemma 3.** For real variables  $\phi$  and  $\gamma$  and any of the positive constants  $\zeta_1, \zeta_2$ , and  $\zeta_3$ , the satisfied inequality is as follows [43]:

$$|\phi|^{\zeta_1} |\gamma|^{\zeta_2} \leq \frac{\zeta_1}{\zeta_1 + \zeta_2} \zeta_3 |\phi|^{\zeta_1 + \zeta_2} + \frac{\zeta_2}{\zeta_1 + \zeta_2} \zeta_3^{-\frac{\zeta_1}{\zeta_2}} |\gamma|^{\zeta_1 + \zeta_2} \tag{4}$$

**Lemma 4.** Consider a nonlinear system  $\dot{\zeta} = f(\zeta)$  with  $\zeta \in R^{n \times 1}$ . On one hand, if there exists a Lyapunov function  $V(\zeta)$  satisfying the following [44]:

$$\dot{V} + h_1 V^{v_3} + h_2 V^{v_4} \leq \Delta_v \tag{5}$$

for some  $h_1 \in R^+, h_2 \in R^+, 0 < v_3 < 1, v_4 \geq 1$ , and  $\Delta_v \in R^+$ , then, the system is finite-time stable.

**Lemma 5.** Consider a nonlinear system  $\dot{\zeta} = f(\zeta)$  with  $\zeta \in R^{n \times 1}$ . If there exists a Lyapunov function  $V(\zeta)$  satisfying the following [45]:

$$\dot{V} \leq -\gamma V^p \tag{6}$$

where  $\gamma > 0, 0 < p < 1$ , then, the system will converge to zero in a finite time  $T \leq \frac{1}{\gamma(1-p)} V^{1-p}$ .

**Assumption 1.** Assuming that the rate of change of the total disturbance to which the system is subjected is bounded,  $|\dot{d}_j| \leq \vartheta_j$  where  $j = p, q, r$ .

**Remark 1.** Although the wind disturbances acting on the quadrotor UAV are readily variable, the energy of the disturbances is also finite; at the same time, although we are unable to measure each of the basic physical parameters of the UAV with any great degree of accuracy, the resulting modeling uncertainty is nearly constant, and the total disturbances to the system can therefore be regarded as signals with a bounded rate of change. In summary, Assumption 1 is reasonable.

**Definition 1.** Define  $|\mathbf{a}|^{m/n} \text{sign}(\mathbf{b}) = [ |a_1|^{m/n} \text{sign}(b_1) \ |a_2|^{m/n} \text{sign}(b_2) \ \dots \ |a_3|^{m/n} \text{sign}(b_3) ]$ , and the vector  $\mathbf{a} \in R^{n \times 1}$  and  $\mathbf{b} \in R^{n \times 1}$ .

The attitude model of the quadrotor UAV includes an attitude kinematics model and an attitude dynamics model, which is modeled based on the Newton–Euler method with the following results:

$$\dot{\mathbf{x}}_1 = \mathbf{A}(\mathbf{x}_1)\mathbf{x}_2 \tag{7}$$

$$\dot{\mathbf{x}}_2 = \mathbf{B}(\mathbf{x}_2) + \mathbf{G}\mathbf{u}_1 + \mathbf{d} \tag{8}$$

$$\mathbf{A}(x_1) = \begin{bmatrix} 1 & \sin \phi \tan \theta & \cos \phi \tan \theta \\ 0 & \cos \phi & -\sin \phi \\ 0 & \sin \phi / \cos \theta & \cos \phi / \cos \theta \end{bmatrix}, \mathbf{G} = \begin{bmatrix} J_x & 0 & 0 \\ 0 & J_y & 0 \\ 0 & 0 & J_z \end{bmatrix}$$

$$\mathbf{B}(x_2) = \begin{bmatrix} \frac{J_y - J_z}{J_x} qr & \frac{J_z - J_x}{J_y} pr & \frac{J_x - J_y}{J_z} pq \end{bmatrix}^T$$

where  $\mathbf{x}_1 = [\phi \ \theta \ \varphi]^T$  and  $\mathbf{x}_2 = [p \ q \ r]^T$  denote the Euler angle and the angular velocity of the body, respectively. Unlike studies [10,12,25,37,38,40], in this paper, there is no equivalence between the rate of change of the Euler angle and the angular velocity of the body.  $\mathbf{G}$  is the moment of inertia matrix.  $\mathbf{d} \in R^3$  denotes the total disturbance of the system.  $\mathbf{u}_1 = [\text{sat}(u_p) \ \text{sat}(u_q) \ \text{sat}(u_r)]^T$ ,  $\text{sat}(\cdot)$  denotes the limiting function in the following form:

$$\text{sat}(u_j) = \begin{cases} u_j & u_j < u_{j,\max} \\ u_{j,\max} & u_j \geq u_{j,\max} \end{cases} \tag{9}$$

### 3. Controller Design

#### 3.1. Anti-Saturation Controller Design Based on Finite-Time Stabilization

Define the error of the system as follows:

$$\mathbf{e}_1 = \mathbf{x}_1 - \mathbf{x}_{1d} - \lambda_1 \tag{10}$$

$$\mathbf{e}_2 = \mathbf{x}_2 - \mathbf{x}_{2d} - \lambda_2 \tag{11}$$

where  $\mathbf{e}_1 = [e_{1,\phi} \ e_{1,\theta} \ e_{1,\varphi}]^T$  corresponds to the angle error of the attitude,  $\mathbf{e}_2 = [e_{2,p} \ e_{2,q} \ e_{2,r}]^T$  corresponds to the velocity error of the angle, and  $\mathbf{x}_{1d} \in R^3$  and  $\mathbf{x}_{2d} \in R^3$  denote the desired attitude angle and the desired angular velocity of the airframe.  $\lambda_1 = [\lambda_{1,\phi}, \lambda_{1,\theta}, \lambda_{1,\varphi}]^T$  and  $\lambda_2 = [\lambda_{2,p}, \lambda_{2,q}, \lambda_{2,r}]^T$  are the states of the anti-saturation auxiliary system.

The anti-saturation auxiliary system in this paper is designed as follows:

$$\dot{\lambda}_1 = -\mathbf{K}_1\lambda_1 - \mathbf{K}_2|\lambda_1|^{m/n}\text{sign}(\mathbf{e}_1) + \mathbf{b}_1\lambda_2 \tag{12}$$

$$\dot{\lambda}_2 = -\mathbf{K}_3\lambda_2 - \mathbf{K}_4|\lambda_2|^{m/n}\text{sign}(\mathbf{e}_2) + \mathbf{G}\Delta\mathbf{u} \tag{13}$$

where  $\Delta\mathbf{u} = \mathbf{u}_1 - \mathbf{u}$ ,  $\mathbf{u}$  is the output of the controller.  $m$  and  $n$  are both positive odd numbers,  $\mathbf{b}_1 \in R^{3 \times 3}$ ,  $\mathbf{K}_1 \in R^{3 \times 3}$ ,  $\mathbf{K}_2 \in R^{3 \times 3}$ ,  $\mathbf{K}_3 \in R^{3 \times 3}$ , and  $\mathbf{K}_4 \in R^{3 \times 3}$  are both diagonal matrices, and the entries in the matrices are all positive constants.

From Equations (12) and (13), it can be seen that the two auxiliary states of the anti-saturation auxiliary system can converge asymptotically to zero when  $\Delta\mathbf{u} = 0$ . Therefore, the anti-saturation system remains inactive in the absence of saturation events; and the two states of the anti-saturation auxiliary system will no longer be zero when  $\Delta\mathbf{u} \neq 0$ . The errors of the system are defined as Equations (10) and (11). In contrast to the common definitions of the errors, the errors of Equations (10) and (11) include the auxiliary system states. Therefore, when saturation occurs, the error will be adaptively adjusted to produce a slightly smaller error, based on which the controller produces a slightly smaller amount of control such that the control command exits the saturated region or is maintained in a shallow saturated region. This is the design idea and control method of the anti-saturation auxiliary system in this paper, and the overall stability of the system will be proved by Lyapunov stability.

Let  $\mathbf{x}_{2d} = \mathbf{A}^{-1}(\mathbf{x}_1)(\dot{\mathbf{x}}_{1d} + \dot{\lambda}_1 + \mathbf{r}_1)$  and substitute this into Equation (8), and combined with Equation (10), we obtain the following:

$$\dot{\mathbf{e}}_1 = \mathbf{r}_1 \tag{14}$$

$\mathbf{r}_1 = -\mathbf{C}_1\mathbf{e}_1 - \mathbf{C}_2|\mathbf{e}_1|^{m/n}\text{sign}(\mathbf{e}_1) + \mathbf{K}_1\lambda_1 + \mathbf{K}_2|\lambda_1|^{m/n}\text{sign}(\mathbf{e}_1) - \mathbf{b}_1\lambda_2$ ,  $\mathbf{C}_1 \in R^{3 \times 3}$  and  $\mathbf{C}_2 \in R^{3 \times 3}$  are both diagonal matrices, and the entries in the matrices are all positive constants.

Differentiation of (11) yields the following:

$$\begin{aligned} \dot{\mathbf{e}}_2 &= \dot{\mathbf{x}}_2 - \dot{\mathbf{x}}_{2d} - \dot{\lambda}_2 \\ &= \mathbf{B}(\mathbf{x}_2) + \mathbf{G}\mathbf{u}_1 + \mathbf{d} - \dot{\mathbf{x}}_{2d} + \mathbf{K}_3\lambda_2 + \mathbf{K}_4|\lambda_2|^{m/n}\text{sign}(\mathbf{e}_2) - \mathbf{G}\Delta\mathbf{u} \\ &= \mathbf{B}(\mathbf{x}_2) + \mathbf{G}\mathbf{u} + \mathbf{d} - \dot{\mathbf{x}}_{2d} + \mathbf{K}_3\lambda_2 + \mathbf{K}_4|\lambda_2|^{m/n}\text{sign}(\mathbf{e}_2) \end{aligned} \tag{15}$$

The designed control law is as follows:

$$\mathbf{u} = \mathbf{G}^{-1}(-\mathbf{B}(\mathbf{x}_2) - \mathbf{d} + \dot{\mathbf{x}}_{2d} - \mathbf{C}_3\mathbf{e}_2 - \mathbf{C}_4|\mathbf{e}_2|^{m/n}\text{sign}(\mathbf{e}_2)) \tag{16}$$

$\mathbf{C}_3 \in R^{3 \times 3}$  and  $\mathbf{C}_4 \in R^{3 \times 3}$  are both diagonal matrices, and the entries in the matrices are all positive constants.

Then, (15) can be rewritten as follows:

$$\dot{\mathbf{e}}_2 = -\mathbf{C}_3\mathbf{e}_2 - \mathbf{C}_4|\mathbf{e}_2|^{m/n}\text{sign}(\mathbf{e}_2) + \mathbf{K}_3\lambda_2 + \mathbf{K}_4|\lambda_2|^{m/n}\text{sign}(\mathbf{e}_2) \tag{17}$$

Therefore, the structure of the finite-time anti-saturation control method (FACM) for the quadrotor UAV attitude system is shown in Figure 1.

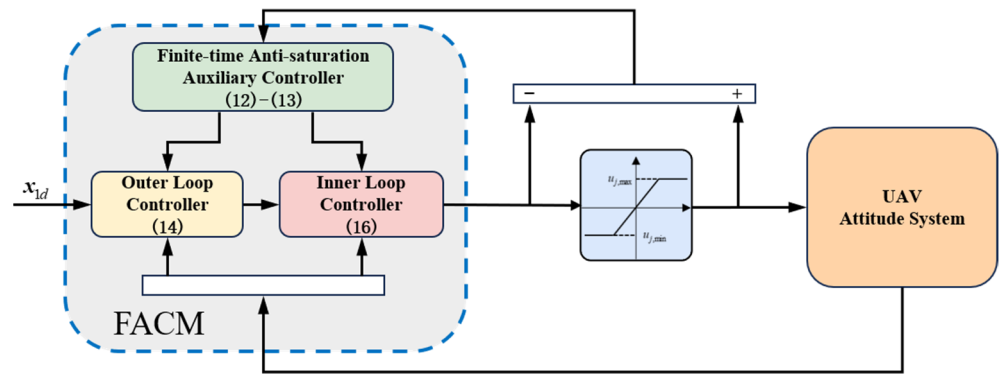


**Figure 1.** The structure of the finite time anti-saturation control method for quadrotor UAV attitude system.

**Theorem 1.** For nonlinear attitude models in the presence of input saturation (7) and (8), under the control law of (16) and the anti-saturation auxiliary system (12) and (13), the quadrotor UAV attitude system angle tracking error will converge to zero in a finite time.

**Proof of Theorem 1.** Because of the similarity of the three-axis attitude system models for quadrotor UAVs, the roll channel is used here as an example to demonstrate that  $e_{1,\phi}$  will converge to zero in a finite time.

The Lyapunov function is chosen with the following form:

$$V_1 = \frac{1}{2}e_{1,\phi}^2 + \frac{1}{2}e_{2,p}^2 \tag{18}$$

Differentiating Equation (18) and combining Equations (14) and (17) gives Equation (19):

$$\begin{aligned} \dot{V}_1 &= e_{1,\phi}\dot{e}_{1,\phi} + e_{2,p}\dot{e}_{2,p} \\ &= -c_{1,1}e_{1,\phi}^2 - c_{2,1}e_{1,\phi}^{(\frac{m+n}{n})} + k_{1,1}e_{1,\phi}\lambda_{1,\phi} + k_{2,1}|\lambda_{1,\phi}|^{(\frac{m}{n})}|e_{1,\phi}| - b_1e_{1,\phi}\lambda_{2,p} - c_{3,1}e_{2,p}^2 - c_{4,1}e_{2,p}^{(\frac{m+n}{n})} \\ &\quad + k_{3,1}e_{2,p}\lambda_{2,p} + k_{4,1}|\lambda_{2,p}|^{(\frac{m}{n})}|e_{2,p}| \\ &= -c_{1,1}e_{1,\phi}^2 - c_{3,1}e_{2,p}^2 - c_{2,1}2^{(\frac{m+n}{2n})}(\frac{1}{2}e_{1,\phi}^2)^{(\frac{m+n}{2n})} - c_{4,1}2^{(\frac{m+n}{2n})}(\frac{1}{2}e_{2,p}^2)^{(\frac{m+n}{2n})} \\ &\quad + k_{1,1}e_{1,\phi}\lambda_{1,\phi} + k_{2,1}|\lambda_{1,\phi}|^{(\frac{m}{n})}|e_{1,\phi}| - b_1e_{1,\phi}\lambda_{2,p} + k_{3,1}e_{2,p}\lambda_{2,p} + k_{4,1}|\lambda_{2,p}|^{(\frac{m}{n})}|e_{2,p}| \end{aligned} \tag{19}$$

It follows from Lemma 2:

$$k_{1,1}e_{1,\phi}\lambda_{1,\phi} \leq \frac{k_{1,1}^2}{2}e_{1,\phi}^2 + \frac{1}{2}\lambda_{1,\phi}^2 \tag{20}$$

$$-b_1e_{1,\phi}\lambda_{2,p} \leq \frac{b_1^2}{2}e_{1,\phi}^2 + \frac{1}{2}\lambda_{2,p}^2 \tag{21}$$

$$k_{3,1}e_{2,p}\lambda_{2,p} \leq \frac{k_{3,1}^2}{2}e_{2,p}^2 + \frac{1}{2}\lambda_{2,p}^2 \tag{22}$$

It follows from Lemma 3:

$$k_{2,1}|\lambda_{1,\phi}|^{(\frac{m}{n})}|e_{1,\phi}| \leq k_{2,1}\frac{m}{m+n}d_{31}|\lambda_{1,\phi}|^{(\frac{m+n}{n})} + k_{2,1}\frac{n}{m+n}d_{31}^{(-\frac{m}{n})}|e_{1,\phi}|^{(\frac{m+n}{n})} \tag{23}$$

$$k_{4,1}|\lambda_{2,p}|^{(\frac{m}{n})}|e_{2,p}| \leq k_{4,1}\frac{m}{m+n}d_{32}|\lambda_{2,p}|^{(\frac{m+n}{n})} + k_{4,1}\frac{n}{m+n}d_{32}^{(-\frac{m}{n})}|e_{2,p}|^{(\frac{m+n}{n})} \tag{24}$$

Substituting Equations (20) and (24) into Equation (19) gives Equation (25):

$$\begin{aligned} \dot{V}_1 \leq & -c_{1,1}e_{1,\phi}^2 - c_{3,1}e_{2,p}^2 - c_{2,1}2^{\left(\frac{m+n}{2n}\right)}\left(\frac{1}{2}e_{1,\phi}^2\right)^{\left(\frac{m+n}{2n}\right)} - c_{4,1}2^{\left(\frac{m+n}{2n}\right)}\left(\frac{1}{2}e_{2,p}^2\right)^{\left(\frac{m+n}{2n}\right)} + \frac{k_{1,1}^2}{2}e_{1,\phi}^2 + \frac{1}{2}\lambda_{1,\phi}^2 \\ & + k_{2,1}\frac{m}{m+n}d_{31}|\lambda_{1,\phi}|^{\left(\frac{m+n}{n}\right)} + k_{2,1}\frac{n}{m+n}d_{31}^{\left(-\frac{m}{n}\right)}|e_{1,\phi}|^{\left(\frac{m+n}{n}\right)} + \frac{b_1^2}{2}e_{1,\phi}^2 + \frac{1}{2}\lambda_{2,p}^2 \\ & + \frac{k_{3,1}^2}{2}e_{2,p}^2 + \frac{1}{2}\lambda_{2,p}^2 + k_{4,1}\frac{m}{m+n}d_{32}|\lambda_{2,p}|^{\left(\frac{m+n}{n}\right)} + k_{4,1}\frac{n}{m+n}d_{32}^{\left(-\frac{m}{n}\right)}|e_{2,p}|^{\left(\frac{m+n}{n}\right)} \end{aligned} \tag{25}$$

Collation yields Equation (26):

$$\begin{aligned} \dot{V}_1 \leq & (-c_{1,1} + \frac{k_{1,1}^2}{2} + \frac{b_1^2}{2})e_{1,\phi}^2 + (-c_{3,1} + \frac{k_{3,1}^2}{2})e_{2,p}^2 + \frac{1}{2}\lambda_{1,\phi}^2 + \lambda_{2,p}^2 \\ & + [-c_{2,1}2^{\left(\frac{m+n}{2n}\right)}\left(\frac{1}{2}e_{1,\phi}^2\right)^{\left(\frac{m+n}{2n}\right)} - c_{4,1}2^{\left(\frac{m+n}{2n}\right)}\left(\frac{1}{2}e_{2,p}^2\right)^{\left(\frac{m+n}{2n}\right)}] \\ & + k_{2,1}\frac{n}{m+n}d_{31}^{\left(-\frac{m}{n}\right)}|e_{1,\phi}|^{\left(\frac{m+n}{n}\right)} + k_{4,1}\frac{n}{m+n}d_{32}^{\left(-\frac{m}{n}\right)}|e_{2,p}|^{\left(\frac{m+n}{n}\right)} \\ & + k_{2,1}\frac{m}{m+n}d_{31}|\lambda_{1,\phi}|^{\left(\frac{m+n}{n}\right)} + k_{4,1}\frac{m}{m+n}d_{32}|\lambda_{2,p}|^{\left(\frac{m+n}{n}\right)} \end{aligned} \tag{26}$$

It follows from (1) of Lemma 1 that

$$\dot{V}_1 \leq -h_1V_1 - h_2V_1^{\left(\frac{m+n}{2n}\right)} + \Xi \tag{27}$$

where  $h_1 = \left\{2c_{1,1} - k_{1,1}^2 - b_1^2, 2c_{3,1} - k_{3,1}^2\right\}$ ,  $h_2 = \left\{c_{2,1}2^{\frac{m+n}{2n}} - k_{2,1}\frac{n}{m+n}d_{31}^{-\frac{m}{n}}2^{\frac{m+n}{2n}}, c_{4,1}2^{\frac{m+n}{2n}} - k_{4,1}\frac{n}{m+n}d_{32}^{-\frac{m}{n}}2^{\frac{m+n}{2n}}\right\}$ ,  $\Xi = \frac{1}{2}\lambda_{1,\phi}^2 + \lambda_{2,p}^2 + k_{2,1}\frac{m}{m+n}d_{31}|\lambda_{1,\phi}|^{\frac{m+n}{n}} + k_{4,1}\frac{m}{m+n}d_{32}|\lambda_{2,p}|^{\frac{m+n}{n}} > 0$ . Choose the appropriate parameters such that  $h_1 > 0$  and  $h_2 > 0$ . According to the finite-time stability theory of Lemma 4, the error of the system will converge to the zero domain in a finite time under the action of the anti-saturation auxiliary system. □

### 3.2. Disturbance Observer Design Based on Finite-Time Stabilization

The observation error is defined as follows:

$$\mathbf{z}_1 = \mathbf{x}_2 - \hat{\mathbf{x}}_2 \tag{28}$$

$$\mathbf{z}_2 = \mathbf{d} - \hat{\mathbf{d}} \tag{29}$$

where  $\mathbf{z}_1 \in R^3$  and  $\mathbf{z}_2 \in R^3$  denote the observation error of the angular velocity of the airframe and the observation error of the total system disturbance, respectively.  $\mathbf{z}_1 = \{z_{1,j}|j = p, q, r\}$ ,  $\mathbf{z}_2 = \{z_{2,j}|j = p, q, r\}$ ,  $\hat{\mathbf{x}}_2 = [\hat{p} \ \hat{q} \ \hat{r}]^T$ , and  $\hat{\mathbf{d}} = [\hat{d}_p \ \hat{d}_q \ \hat{d}_r]^T$  are estimates of the angular velocity of the system and the total system disturbance.

For Equation (8), inspired by the studies [31,40], the finite-time disturbance observer designed in this paper is as follows:

$$\dot{\hat{\mathbf{x}}}_2 = \mathbf{B}(\mathbf{x}_2) + \mathbf{G}\mathbf{u}_1 + \hat{\mathbf{d}} + \mathbf{A}_1|\mathbf{z}_1|^{\frac{1}{2}}\tanh(\mathbf{kz}_1) \tag{30}$$

$$\dot{\hat{\mathbf{d}}} = \mathbf{A}_2\tanh(\mathbf{kz}_1) \tag{31}$$

$\tanh(\cdot)$  is the hyperbolic tangent function, and it effectively reduces the chattering phenomenon of the observation output.  $\mathbf{A}_1$ ,  $\mathbf{A}_2$ , and  $\mathbf{k}$  are the matrices of scale factors.  $\mathbf{A}_1 = \text{diag}(a_{1,p}, a_{1,q}, a_{1,r})$ ,  $\mathbf{A}_2 = \text{diag}(a_{2,p}, a_{2,q}, a_{2,r})$ ,  $\mathbf{k} = \text{diag}(k_p, k_q, k_r)$ ,  $|\mathbf{z}_1|^{\frac{1}{2}} = \text{diag}(|z_{1,p}|^{\frac{1}{2}}, |z_{1,q}|^{\frac{1}{2}}, |z_{1,r}|^{\frac{1}{2}})$ ,  $a_{i,j} > 0$ ,  $k_j > 0$ , and  $i = 1, 2$ . Compared with the FDOs in the studies [31,40], the FDO in this paper has fewer adjustable parameters and effectively improves the chattering phenomenon of the output results of the existing FDOs by designing a continuous-type observer.

By combining Equations (8), (28) and (29), we obtain the following:

$$\dot{\mathbf{z}}_1 = -\mathbf{A}_1|\mathbf{z}_1|^{\frac{1}{2}}\tanh(\mathbf{kz}_1) + \mathbf{z}_2 \tag{32}$$

$$\dot{z}_2 = -A_2 \tanh(kz_1) + \dot{d} \tag{33}$$

Equations (32) and (33) are the dynamic equations for the observer error.

Therefore, the structure of the finite-time disturbance observer and anti-saturation control method for the quadrotor UAV attitude system is shown in Figure 2.

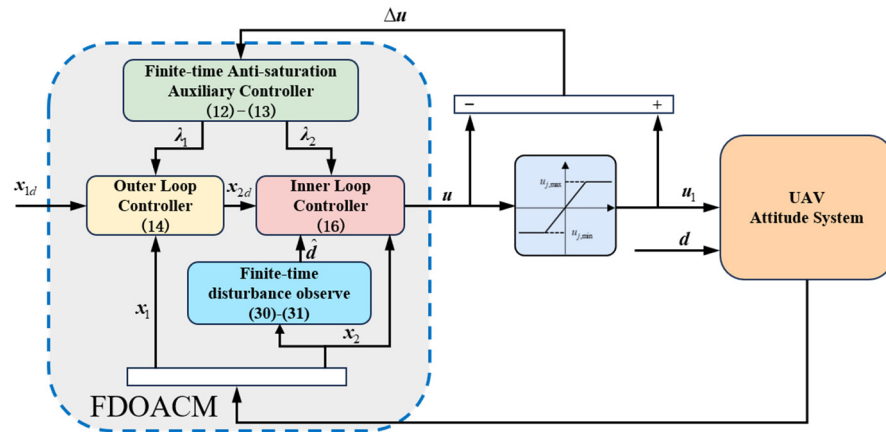


**Figure 2.** The structure of finite-time disturbance observer and anti-saturation control method for quadrotor UAV attitude system.

**Theorem 2.** *If the total disturbance suffered by the quadrotor UAV satisfies Assumption 1, and at the same time, the matrix  $\Pi$  is made to satisfy the condition of the positive definite symmetric matrix by reasonable parameter settings, the designed FDO (30) and (31) will effectively estimate the total disturbance, and the output error of the FDO will converge to zero in a finite time.*

$$\Pi = \begin{bmatrix} a_{1,p}rP_{11} - 2a_{1,p}a_{2,p}r - 2a_{1,p}\vartheta_p & -\frac{1}{2}(P_{11} + a_{1,p}^2r + 4a_{2,p}r + 4\vartheta_p) \\ -\frac{1}{2}(P_{11} + a_{1,p}^2r + 4a_{2,p}r + 4\vartheta_p) & a_{1,p} \end{bmatrix} \tag{34}$$

**Proof of Theorem 2.** Similarly, without loss of generality, the roll channel is used here as an example to demonstrate that  $z_{1,\phi}$  will converge to zero in a finite time.

Set the vector  $\Psi = [sign(z_{1,p})|z_{1,p}|^{\frac{1}{2}} \quad z_{2,p}]^T$  and define the Lyapunov function as:

$$V_{FDO} = \Psi^T P \Psi = P_{11}|z_{1,p}| - 2a_{1,p}z_{2,p}sign(z_{1,p})|z_{1,p}|^{\frac{1}{2}} + 2z_{2,p}^2 \tag{35}$$

$P = \begin{bmatrix} a_{1,p}^2 + a_{2,p}^2 & -a_{1,p} \\ -a_{1,p} & 2 \end{bmatrix}$ . It is clear that the matrix  $P$  is a positive definite real symmetric matrix, and hence, Equation (35) satisfies the conditions of the Lyapunov function.

Derivation of Equation (35):

$$\dot{V}_{FDO} = P_{11} \frac{z_{1,p}}{|z_{1,p}|} \dot{z}_{1,p} - 2a_{1,p} \dot{z}_{2,p} sign(z_{1,p}) |z_{1,p}|^{\frac{1}{2}} - a_{1,p} z_{2,p} |z_{1,p}|^{-\frac{1}{2}} \dot{z}_{1,p} + 4z_{2,p} \dot{z}_{2,p} \tag{36}$$

Substituting Equation (32) into Equation (35):

$$\begin{aligned} \dot{V}_{FDO} = & P_{11} \frac{z_{1,p}}{|z_{1,p}|} (-a_{1,p} |z_{1,p}|^{\frac{1}{2}} \tanh(k_p z_{1,p}) + z_{2,p}) + 4z_{2,p} (-a_{2,p} \tanh(k_p z_{1,p}) + \dot{d}_p) \\ & - 2a_{1,p} sign(z_{1,p}) |z_{1,p}|^{\frac{1}{2}} (-a_{2,p} \tanh(k_p z_{1,p}) + \dot{d}_p) - a_{1,p} z_{2,p} |z_{1,p}|^{-\frac{1}{2}} (-a_{1,p} |z_{1,p}|^{\frac{1}{2}} \\ & \tanh(k_p z_{1,p}) + z_{2,p}) \end{aligned} \tag{37}$$

Since  $\tanh(kx) = rsign(x)$ , where  $r \in (0, 1)$ , rewriting Equation (37) gives the following:

$$\begin{aligned} \dot{V}_{FDO} &= P_{11} \frac{z_{1,p}}{|z_{1,p}|} (-a_{1,p}r|z_{1,p}|^{\frac{1}{2}} \text{sign}(z_{1,p}) + z_{2,p}) - 2a_{1,p} \text{sign}(z_{1,p})|z_{1,p}|^{\frac{1}{2}} (-a_{2,p}r \text{sign}(z_{1,p}) + \dot{d}_p) \\ &\quad - a_{1,p}z_{2,p}|z_{1,p}|^{-\frac{1}{2}} (-a_{1,p}r|z_{1,p}|^{\frac{1}{2}} \text{sign}(z_{1,p}) + z_{2,p}) + 4z_{2,p}(-a_{2,p}r \text{sign}(z_{1,p}) + \dot{d}_p) \\ &= -a_{1,p}rP_{11}|z_{1,p}|^{\frac{1}{2}} + P_{11} \frac{z_{1,p}}{|z_{1,p}|} z_{2,p} + 2a_{1,p}a_{2,p}r|z_{1,p}|^{\frac{1}{2}} - 2a_{1,p} \text{sign}(z_{1,p})\dot{d}_p + a_{1,p}^2 r z_{2,p} \text{sign}(z_{1,p}) \\ &\quad - a_{1,p}z_{2,p}^2|z_{1,p}|^{-\frac{1}{2}} - 4a_{2,p}r z_{2,p} \text{sign}(z_{1,p}) + 4z_{2,p}\dot{d}_p \end{aligned} \tag{38}$$

Since  $|\text{sign}(x)| \leq 1$ ,  $\text{sign}(x) \leq 1$ ,  $-\text{sign}(x) \leq 1$ :

$$\begin{aligned} \dot{V}_{FDO} &\leq -a_{1,p}rP_{11}|z_{1,p}|^{\frac{1}{2}} + P_{11} \frac{z_{1,p}}{|z_{1,p}|} z_{2,p} + 2a_{1,p}a_{2,p}r|z_{1,p}|^{\frac{1}{2}} + 2a_{1,p}|z_{1,p}|^{\frac{1}{2}}\dot{d}_p + a_{1,p}^2 r z_{2,p} \\ &\quad - a_{1,p}z_{2,p}^2|z_{1,p}|^{-\frac{1}{2}} + 4a_{2,p}r z_{2,p} + 4z_{2,p}\dot{d}_p \end{aligned} \tag{39}$$

By Assumption 1,  $|\dot{d}_p| \leq \vartheta_p$ ,  $z_{1,p} \leq |z_{1,p}|$  and  $z_{2,p} \leq |z_{2,p}|$ , we obtain the following:

$$\begin{aligned} \dot{V}_{FDO} &\leq -a_{1,p}rP_{11}|z_{1,p}|^{\frac{1}{2}} + P_{11}|z_{2,p}| + 2a_{1,p}a_{2,p}r|z_{1,p}|^{\frac{1}{2}} + 2a_{1,p}|z_{1,p}|^{\frac{1}{2}}\vartheta_p + a_{1,p}^2 r|z_{2,p}| \\ &\quad - a_{1,p}z_{2,p}^2|z_{1,p}|^{-\frac{1}{2}} + 4a_{2,p}r|z_{2,p}| + 4|z_{2,p}|\vartheta_p \\ &= -\frac{1}{|z_{1,p}|^{\frac{1}{2}}} [a_{1,p}rP_{11}|z_{1,p}| - P_{11}|z_{2,p}||z_{1,p}|^{\frac{1}{2}} - 2a_{1,p}a_{2,p}r|z_{1,p}| - 2a_{1,p}|z_{1,p}|\vartheta_p \\ &\quad - a_{1,p}^2 r|z_{2,p}||z_{1,p}|^{\frac{1}{2}} + a_{1,p}z_{2,p}^2 - 4a_{2,p}r|z_{2,p}||z_{1,p}|^{\frac{1}{2}} - 4|z_{2,p}||z_{1,p}|^{\frac{1}{2}}\vartheta_p] \end{aligned} \tag{40}$$

By defining  $\Xi = \begin{bmatrix} \text{sign}(z_{1,p})|z_{1,p}|^{\frac{1}{2}} & |z_{2,p}| \end{bmatrix}^T$ , then Equation (40) can be rewritten as follows:

$$\begin{aligned} \dot{V}_{FDO} &\leq -\frac{1}{|z_{1,p}|^{\frac{1}{2}}} \Xi^T \begin{bmatrix} a_{1,p}rP_{11} - 2a_{1,p}a_{2,p}r - 2a_{1,p}\vartheta_p & -\frac{1}{2}(P_{11} + a_{1,p}^2 r + 4a_{2,p}r + 4\vartheta_p) \\ -\frac{1}{2}(P_{11} + a_{1,p}^2 r + 4a_{2,p}r + 4\vartheta_p) & a_{1,p} \end{bmatrix} \Xi \\ &= -\frac{1}{|z_{1,p}|^{\frac{1}{2}}} \Xi^T \Pi \Xi \end{aligned} \tag{41}$$

Because  $\Xi^T \Xi = \Psi^T \Psi$ , we obtain the following:

$$\dot{V}_{FDO} \leq -\frac{1}{|z_{1,p}|^{\frac{1}{2}}} \Xi^T \Pi \Xi \leq -\frac{\lambda_{\min}(\Pi)}{|z_{1,p}|^{\frac{1}{2}}} \Psi^T \Psi \leq -\frac{\lambda_{\min}(\Pi)V_{FDO}}{\lambda_{\max}(P)|z_{1,p}|^{\frac{1}{2}}} \tag{42}$$

Because  $\|\Psi^T \Psi\| \geq |z_{1,p}|^{\frac{1}{2}}$ ,  $\frac{V_{FDO}^{\frac{1}{2}}}{\sqrt{\lambda_{\min}(P)}} \geq \|\Psi^T \Psi\|$ , we obtain the following:

$$\frac{1}{|z_{1,p}|^{\frac{1}{2}}} \geq \frac{\sqrt{\lambda_{\min}(P)}}{V_{FDO}^{\frac{1}{2}}} \tag{43}$$

Substituting Equation (43) into Equation (42) yields the following:

$$\dot{V}_{FDO} \leq -\frac{\lambda_{\min}(\Pi)\sqrt{\lambda_{\min}(P)}}{\lambda_{\max}(P)} V_{FDO}^{\frac{1}{2}} \tag{44}$$

From Lemma 5, the observation error of the roll channel will converge to zero at time  $T_p$ , and  $T_p$  satisfies the following relation:

$$T_p \leq \frac{2\lambda_{\max}(P)}{\lambda_{\min}(\Pi)\sqrt{\lambda_{\min}(P)}} V_{FDO}^{\frac{1}{2}} \tag{45}$$

Thus, the observer is effective in estimating the external disturbance, and the proof ends.  $\square$

In order to demonstrate the continuity of the observer in this paper, the observer in this paper is compared with the observer in the study [31]. To ensure the uniformity of the comparison conditions, two observers are used to observe the system of Example 1 in the study [31]. The observer designed based on the method of this paper is shown in Equation (46). The observer in the study [31] is shown in Equation (47). The comparison results are shown in Figure 3.

$$\begin{cases} \dot{\hat{x}} = -x + \hat{d} + a_1|x - \hat{x}|^{\frac{1}{2}}\tanh(k(x - \hat{x})) \\ \dot{\hat{d}} = a_2|x - \hat{x}|^{\frac{1}{2}}\tanh(k(x - \hat{x})) \end{cases} \quad (46)$$

$$\begin{cases} \dot{\hat{x}}_1 = -x_1 + \hat{x}_2 + Lc_1(x_1 - \hat{x}_1)^{r_2}, \\ \dot{\hat{x}}_2 = \hat{x}_3 + L^2c_2(x_1 - \hat{x}_1)^{r_3}, \\ \dot{\hat{x}}_3 = \hat{x}_4 + L^3c_3(x_1 - \hat{x}_1)^{r_4}, \\ \dot{\hat{x}}_4 = -\text{Sat}_B(\hat{x}_3) + L^4c_4(x_1 - \hat{x}_1)^{r_5} \end{cases} \quad (47)$$

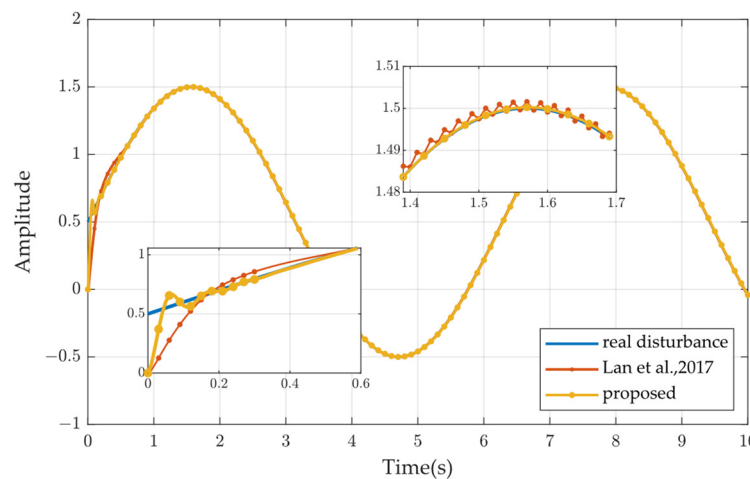


Figure 3. Compare observations with study [31].

From the results, it can be seen that, at the beginning, the outputs of both observers are overshooting because the initial value of the observer output is zero by default, and the observer designed in this paper has a faster response speed. At the peaks and troughs, the observed curves of the study [31] show chattering, while the observer designed in this paper does not show the chattering phenomenon.

**Remark 2.** In the comparison process,  $a_1 = 5$ ,  $a_2 = 20$ , and  $k = 200$ , the parameters of Equation (47) are set as in the study [31].

#### 4. Simulation and Analysis

The algorithm proposed in this chapter is simulated using Simulink, and two scenarios are considered for simulation verification.

Scenario 1: In order to fully verify the control effect of the anti-saturation auxiliary controller, the proposed finite-time anti-saturation control method (FACM) and nonlinear dynamic inversion (NDI) are applied. It is assumed that the disturbance is known during the simulation process, and the UAV needs to perform a large angle maneuver in a short period at this time, which causes the control output of the flight system controller to reach the saturation state.

The desired attitude is as follows:

$$\text{roll}_d = 0.32 \sin(1.3t + 0.5\pi) + 0.3, \text{pitch}_d = 0.32 \sin(1.3t) + 0.5, \text{yaw}_d = 0$$

The initial angle of the drone is  $\Theta_0 = [0; 0; 0.3]^T$  rad. The moment saturation intervals for the roll and pitch channels are  $[-0.03, 0.03]$  N · m. The moment saturation interval of the yaw channel is  $[-0.005, 0.005]$  N · m. The moment of inertia matrix is  $\mathbf{G} = \text{diag}(0.004021, 0.004021, 0.006564)$  kg · m<sup>2</sup>. The controller parameters are shown below:

$$\mathbf{C}_1 = \begin{bmatrix} 3.75 & 0 & 0 \\ 0 & 3.75 & 0 \\ 0 & 0 & 3.75 \end{bmatrix}, \mathbf{C}_3 = \begin{bmatrix} 15 & 0 & 0 \\ 0 & 15 & 0 \\ 0 & 0 & 15 \end{bmatrix}, \mathbf{C}_2 = \mathbf{C}_4 = \mathbf{I}_{3 \times 3}$$

$$\mathbf{K}_1 = \begin{bmatrix} 5 & 0 & 0 \\ 0 & 5 & 0 \\ 0 & 0 & 5 \end{bmatrix}, \mathbf{K}_2 = \mathbf{I}_{3 \times 3}, \mathbf{K}_3 = \begin{bmatrix} 2 & 0 & 0 \\ 0 & 2 & 0 \\ 0 & 0 & 2 \end{bmatrix}, \mathbf{K}_4 = \begin{bmatrix} 0.1 & 0 & 0 \\ 0 & 0.1 & 0 \\ 0 & 0 & 0.1 \end{bmatrix}, \mathbf{b}_1 = \begin{bmatrix} 0.05 & 0 & 0 \\ 0 & 0.05 & 0 \\ 0 & 0 & 0.05 \end{bmatrix}$$

$$m = 99, n = 103, \lambda_{1,0} = [0 \ 0 \ 0]^T, \lambda_{2,0} = [0 \ 0 \ 0]^T$$

The simulation results are shown in Figures 4–6. Figure 4 shows the moments applied to the quadrotor UAV. It is obvious from the figure that, under both control algorithms, the controller output saturation occurs. At the initial moment, compared to the algorithm without an anti-saturation auxiliary controller, the FACM algorithm is in the saturated state for less time, although the saturation of the output moment also occurs. Therefore, the FACM algorithm proposed in this paper minimizes the duration of control moment saturation.

Figure 5 shows the attitude tracking results of the quadrotor UAV. In general, the attitude tracking error tends to become zero around 2.5 s with or without the anti-saturation auxiliary system in the case of known disturbance, so both control methods achieve good attitude tracking results. At the beginning of the simulation, the errors of both control methods are larger before 2.5 s because the initial attitude angle is not consistent with the desired attitude. In the 0~2.5 s interval, when there is no anti-saturation auxiliary system, both the roll channel and the pitch channel can keep up with the desired attitude faster, while the FACM algorithm designed in this paper lags slightly; in the yaw channel, when there is no anti-saturation auxiliary system, it has a larger overshooting amount although it has a shorter rise time; and the FACM algorithm achieves an asymptotic convergence of the yaw angle, and the regulation of the yaw angle is slightly slower, but it is also in the range of 2.5 s. The FACM algorithm achieves an asymptotic convergence of the yaw angle, and the adjustment time is a little slower, but it also makes the tracking error converge to zero in about 2.5 s. The reason for this phenomenon is that, at the beginning, due to the existence of a large error, the control moment reaches the saturation state, as can be seen from Figure 4, and for the algorithm without the anti-saturation auxiliary controller, the control volume is in the saturation state for a longer time, and the time of the maximum torque effect is also longer, so that it can track the desired attitude faster, but at this point, there is also a consequent overshooting, and the overshooting volume of the roll channel and yaw channel is especially obvious; on the contrary, in the FACM algorithm, due to the introduction of the anti-saturation auxiliary system based on the control algorithm, when the saturation phenomenon occurs, the auxiliary states of the anti-saturation system are changed, which reduce the angular tracking error, and thus shorten the time of the control moment in the saturated state, and the time of the maximum torque action is even shorter, so the FACM algorithm cannot track the desired attitude very quickly in the initial stage.

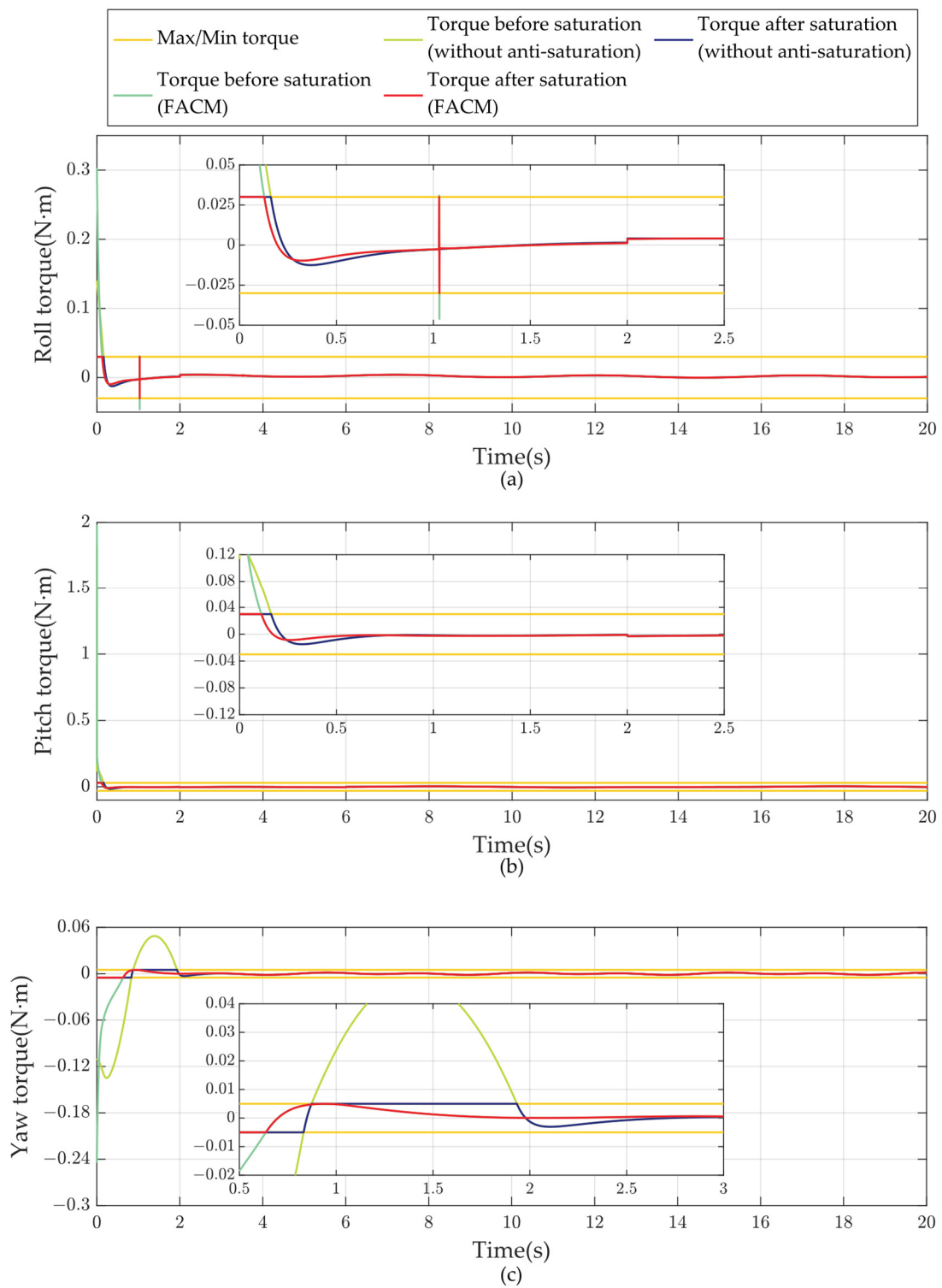


**Figure 4.** Control moment comparison result. Subplot (a–c) are the torques of the roll, pitch, and yaw channels, respectively, under different control algorithms.

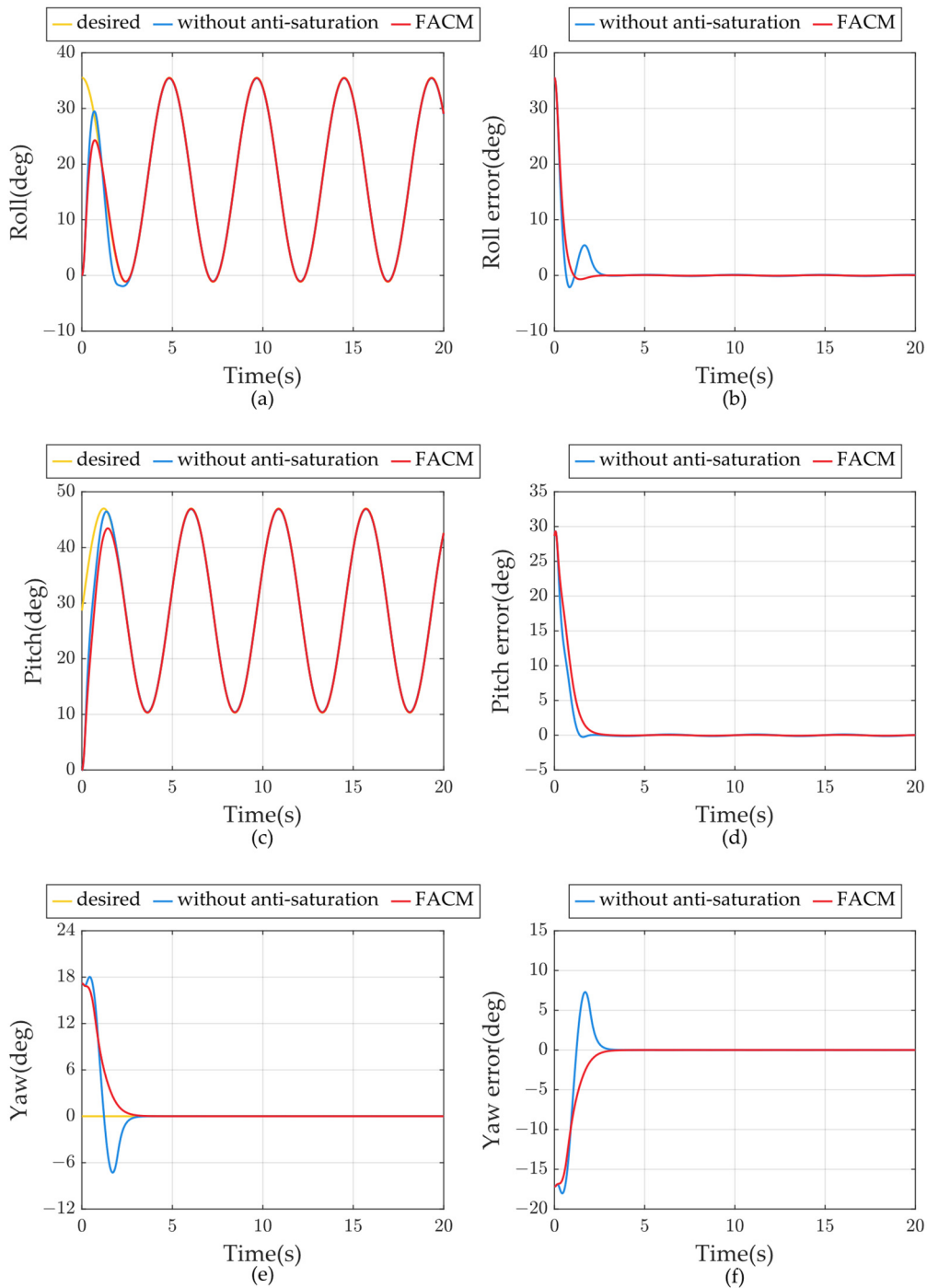


**Figure 5.** Attitude tracking results in comparison. (a,b) denote the attitude tracking results and tracking errors of the roll channel. (c,d) denote the attitude tracking results and tracking errors of the pitch channel. (e,f) denote the attitude tracking results and tracking errors of the yaw channel.

Figure 6 shows the variation in the states of the anti-saturation auxiliary system. It can be seen from the figure that the states a and b change abruptly from zero at the very beginning due to the saturation phenomenon at the initial stage. After that, with the progressive reduction in the angular tracking error, the control moments also decrease, and the system is no longer saturated, so the input of the anti-saturation auxiliary system becomes zero, and the states of the anti-saturation auxiliary system also converge to zero in a finite time.

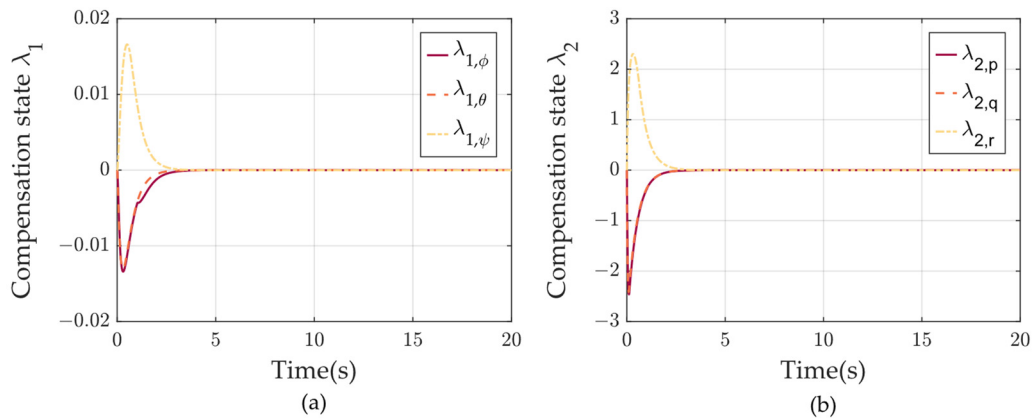


**Figure 6.** Anti-saturation auxiliary system compensation states change results. (a) denotes the amount of compensation state  $\lambda_1$ . (b) denotes the amount of compensation state  $\lambda_2$ .

Scenario 2: In order to be closely related to the real environment, in Scenario 2, it is assumed that the external disturbance is unknown, and it is controlled by using the proposed finite-time disturbance observer and anti-saturation control method (FDOACM); at the same time, to verify the effectiveness of the proposed algorithm, the FACM algorithm and the composite continuous fast nonsingular terminal sliding mode (CCFNTSM) algorithm [46] are also applied to the attitude system model of the quadrotor UAV.

The total disturbance settings to which the system is subjected are shown in Table 1.

**Table 1.** Total disturbance to the system.

Disturbance (rad/s <sup>2</sup> )	$0 \leq t \leq 2$	$2 < t \leq 6$	$t > 6$
$d_p$	−3	−8	$−6 − 2 \sin(0.1\pi t)$
$d_q$	5	6	$2 + 10 \sin(0.2\pi t)$
$d_r$	−3	−6	$−6 − 2.4 \sin(0.25\pi t)$

The desired attitude is consistent with Scenario 1. The initial angle is  $\Theta_0 = [0; 0; 0.3]^T$  rad. The moment saturation intervals for the roll, pitch, and yaw channels are all  $[−0.5, 0.5]$  N·m. The observer parameters are as follows:

$$A_1 = \begin{bmatrix} 100 & 0 & 0 \\ 0 & 100 & 0 \\ 0 & 0 & 100 \end{bmatrix}, A_2 = \begin{bmatrix} 300 & 0 & 0 \\ 0 & 300 & 0 \\ 0 & 0 & 300 \end{bmatrix}, k = \begin{bmatrix} 100 & 0 & 0 \\ 0 & 100 & 0 \\ 0 & 0 & 100 \end{bmatrix}$$

The simulation results are shown in Figures 7–9. Figure 7 shows the UAV attitude tracking results under different control algorithms and unknown disturbance. Since the FACM algorithm has no disturbance observer module, the control effects of this algorithm are the worst among the three; the CCFNTSM algorithm achieves the accurate tracking of the desired attitude in three axes; in the pitch channel and the yaw channel, for the attitude tracking error, although converging to zero in about 1 s, overshooting phenomenon occurs in the process of convergence; in the roll channel, the error convergence effect is better, and the error convergence is achieved in about 1 s with no overshooting phenomenon. Under the control of the FDOACM algorithm, the accurate tracking of the attitude is also achieved; in the roll channel, the control effects of the FDOACM and the CCFNTSM are the same, and the convergence time of the pitch tracking error is nearly the same; in the pitch channel, the convergence time of the FDOACM control algorithm is slightly longer than that of the CCFNTSM algorithm; in the yaw channel, the FDOACM algorithm has a much lower amount of overshooting.

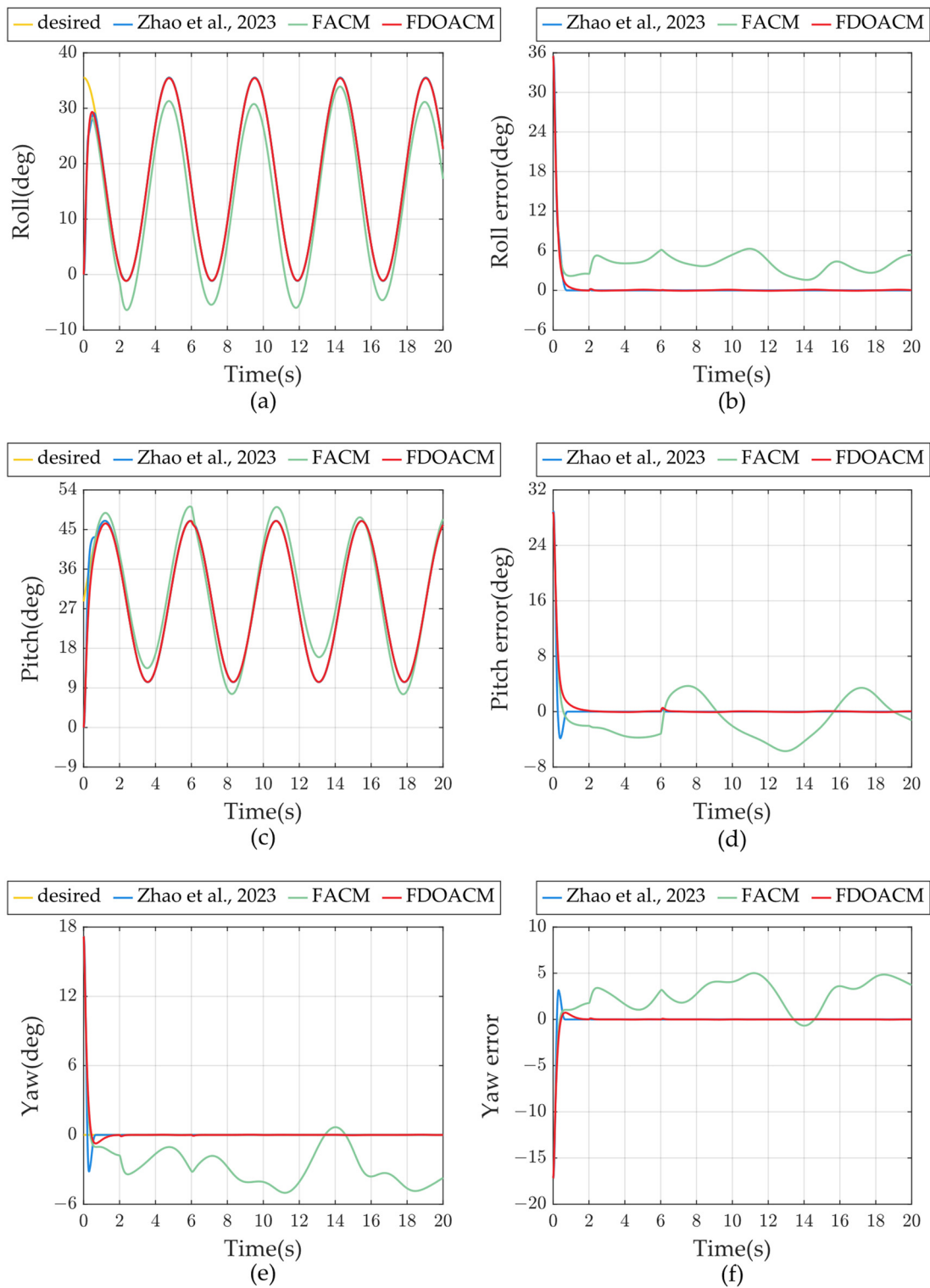


**Figure 7.** Comparison of attitude tracking results in the disturbance situation with study [46] and FACM. (a,b) denote the attitude tracking results and tracking errors of the roll channel. (c,d) denote the attitude tracking results and tracking errors of the pitch channel. (e,f) denote the attitude tracking results and tracking errors of the yaw channel.

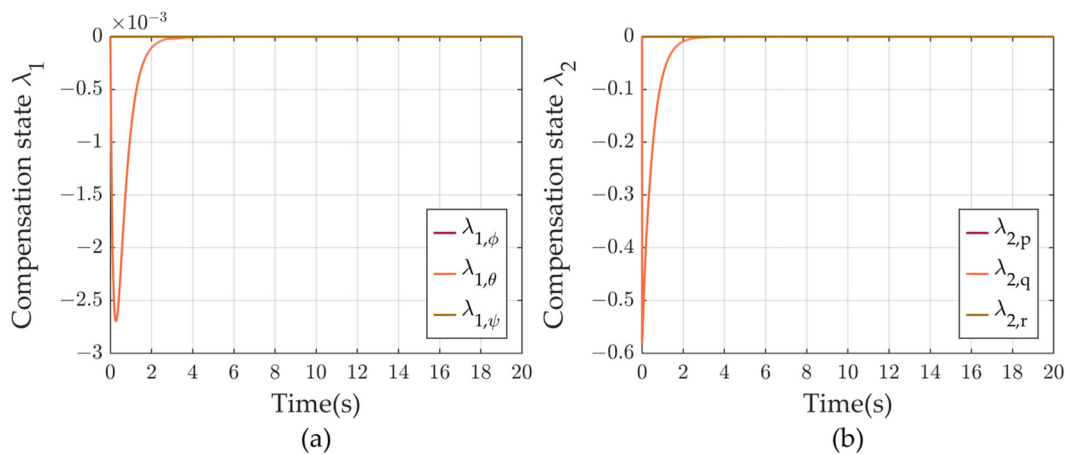


**Figure 8.** Anti-saturation auxiliary system compensation states change results with disturbance observer. (a) denotes the amount of compensation state  $\lambda_1$ . (b) denotes the amount of compensation state  $\lambda_2$ .

Figure 8 shows the change in the states of the anti-saturation auxiliary system. From the figure, it can be seen that the pitch channel triggered the anti-saturation auxiliary controller, so the compensation state of the pitch channel changed. In contrast, the roll channel and the yaw channel show no change in the compensation state quantity because there is no saturation phenomenon.

From the figure, it can be seen that, in the initial stage of simulation, the control effects of the FDOACM algorithm in this paper are not as good as those of the CCFNTSM algorithm for the following reasons: due to the attitude angle error being larger in the initial moments, it triggers the anti-saturation controller in the FDOACM, which leads to the torque maintaining saturation for a shorter time; however, from the subsequent overall results, with the anti-saturation auxiliary state converging to zero, the controller designed in this paper is still able to outperform and give a better control performance. From Figures 7 and 8, it can be seen that the convergence times of the compensated states and the error are almost the same, and the values of the compensated states are in the same order of magnitude as the error, so it can be judged that the slower convergence time is due to the compensated states.

Figure 9 represents the results of different observers for the disturbance. In the initial stage of the simulation, the observer of the study [46] shows an extremely sharp change, especially in Figure 9b, the observer result changes abruptly from the initial zero to about  $420 \text{ rad/s}^2$ , and then gradually converges; when the subsequent disturbance shows a large sudden change, the output of the observer of the study [46] also changes abruptly, and the observation results approximate the actual disturbance in a linear relationship, and a certain degree of an overshooting phenomenon occurs. It can also be seen that, although the observation of the study [46] can quickly observe the external disturbance, there is still a small inconsistency in the observation results, which does not completely achieve the accurate estimation of the external disturbance. On the contrary, the observation results of the FDOCAM control algorithm, whether in the initial stage of the simulation, or the disturbance of a sudden change, the FDO designed in this paper does not appear to be a sudden change, and there is no overshooting phenomenon, and the observation error can be stabilized near the zero domain without chattering; although the algorithm's disturbance observation error is exponentially convergent, the speed of convergence is not worse than that of the study [46], and in Figure 9a,c, the convergence speed of the FDOCAM is more rapid.

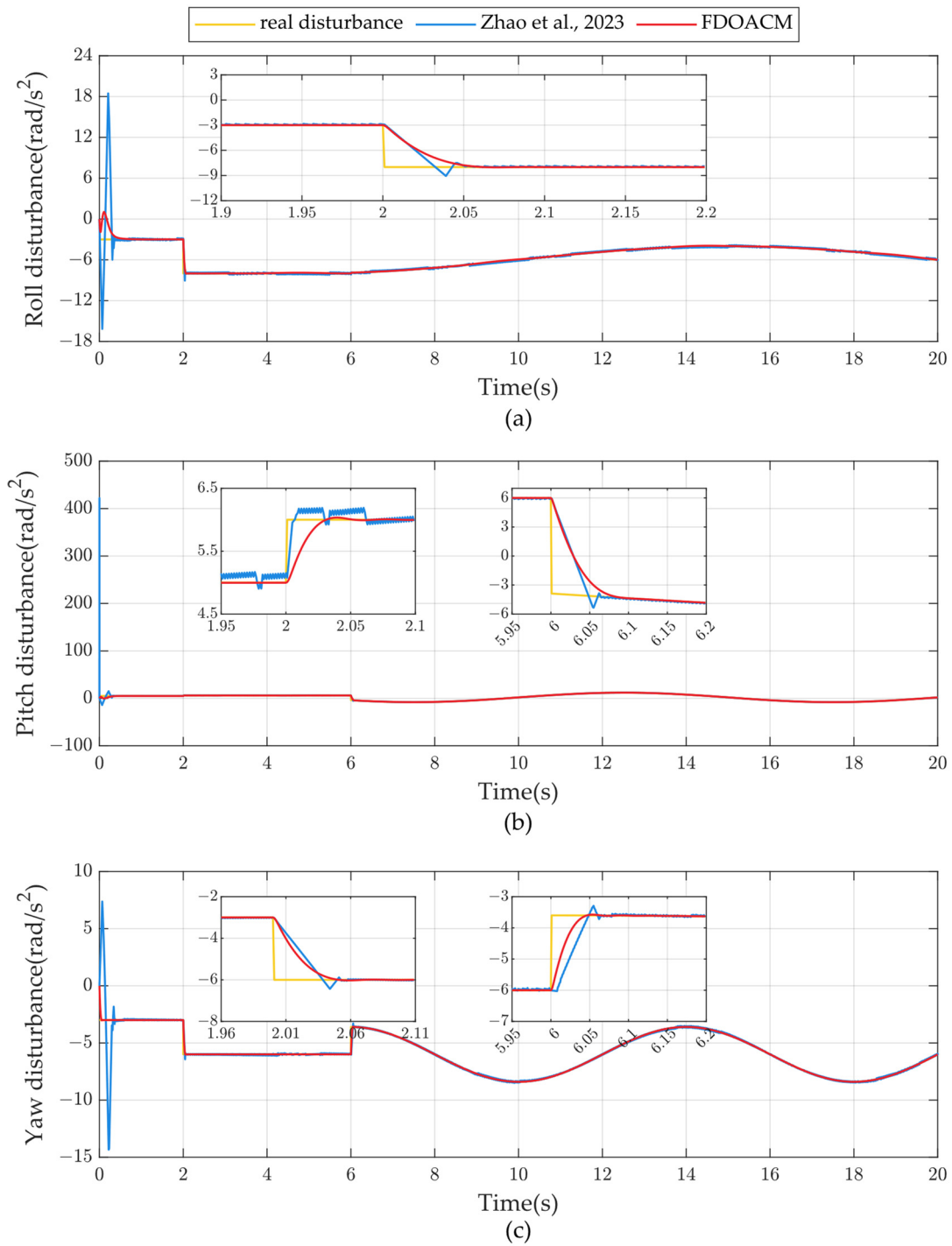


**Figure 9.** Comparison of observations with literature [46]. (a–c) denote the disturbance estimation results of the two algorithms for the roll, pitch, and yaw channels, respectively.

### 5. Conclusions

In this paper, a nonlinear dynamic inversion control algorithm based on a finite-time disturbance observer and an anti-saturation auxiliary system is designed for the actuator saturation problem and the unknown disturbance in the attitude tracking process of a UAV. Firstly, for the actuator saturation problem, a finite-time anti-saturation strategy is proposed, and the anti-saturation control of the actuator is achieved by constructing a second-order anti-saturation auxiliary controller and introducing an anti-saturation auxiliary state in the system error term. Secondly, for the problem of unknown disturbance, an FDO is

designed, and a hyperbolic tangent function is introduced into the disturbance observer, which effectively improves the jitter phenomenon of the existing finite-time disturbance observer. Finally, simulation tests show that the algorithm proposed in this paper can achieve accurate attitude tracking control, which not only reduces the time that the actuator is in the saturation state but also quickly estimates the unknown disturbance to which the system is subjected.

Future research will be carried out for the case where the saturation boundary is unknown and time-varying. Currently, we have only performed Software-in-the-Loop (SIL) simulation, and we will follow up with Hardware-in-the-Loop (HIL) simulation work to further validate the control effect of the algorithm. In addition, our current study focuses on attitude control, on which we plan to design position controllers in the future with an aim to autonomize navigation tasks for UAVs. Due to the importance of the field of intelligent control, we will also introduce intelligent control into our research in our subsequent work.

**Author Contributions:** Conceptualization, Z.Z. and X.L.; Methodology, Z.Z.; Software, Z.Z.; Validation, Z.Z., X.L. and L.Z.; Formal Analysis, Z.Z.; Resources, Z.Z.; Data Curation, Z.Z.; Writing—Original Draft Preparation, Z.Z.; Writing—Review and Editing, Z.Z.; Visualization, Z.Z.; Supervision, X.L. and L.Z.; Project Administration, Z.Z. All authors have read and agreed to the published version of the manuscript.

**Funding:** This research received no external funding.

**Institutional Review Board Statement:** Not applicable.

**Informed Consent Statement:** Not applicable.

**Data Availability Statement:** The original contributions presented in the study are included in the article, further inquiries can be directed to the corresponding author.

**Conflicts of Interest:** The authors declare no conflicts of interest.

## References

1. Erdelj, M.; Krol, M.; Natalizio, E. Wireless sensor networks and multi-UAV systems for natural disaster management. *Comput. Netw.* **2017**, *124*, 72–86. [[CrossRef](#)]
2. Khan, M.A.; Ectors, W.; Bellemans, T.; Janssens, D.; Wets, G. UAV-based traffic analysis: A universal guiding framework based on literature survey. *Transp. Res. Proc.* **2017**, *22*, 541–550. [[CrossRef](#)]
3. dos Santos, S.; Givigi, S.; Nascimento, C. Autonomous Construction of multiple structures using learning automata: Description and experimental validation. *IEEE Syst. J.* **2014**, *9*, 1376–1387. [[CrossRef](#)]
4. Altuğ, E.; Ostrowski, J.P.; Taylor, C.J. Control of a quadrotor helicopter using dual camera visual feedback. *Int. J. Robot. Res.* **2005**, *24*, 329–341. [[CrossRef](#)]
5. Lin, P.; Chen, S.; Wang, X. An improved backstepping based controller with integrators for the quadrotor. In Proceedings of the 2015 34th Chinese Control Conference (CCC), Hangzhou, China, 28–30 July 2015; pp. 545–550.
6. Xu, G.; Zhou, M. Modified adaptive flight control of quadrotor based on single neuron PID. In Proceedings of the 2013 IEEE Third International Conference on Information Science and Technology (ICIST), Yangzhou, China, 23–25 March 2013; pp. 313–316.
7. Kazim, M.; Azar, A.T.; Koubaa, A.; Zaidi, A. Disturbance-rejection-based optimized robust adaptive controllers for UAVs. *IEEE Syst. J.* **2021**, *15*, 3097–3108. [[CrossRef](#)]
8. Reyes-Valeria, E.; Enriquez-Caldera, R.; Camacho-Lara, S.; Guichard, J. LQR control for a quadrotor using unit quaternions: Modeling and simulation. In Proceedings of the CONIELECOMP 2013, 23rd International Conference on Electronics, Communications and Computing, Cholula, Mexico, 11–13 March 2013; pp. 172–178.
9. Guo, Y.; Wu, M.; Tang, K.; Wang, X. Integral back-stepping algorithm for designing the quadrotor aircraft controller. *Chin. J. Intell. Sci. Technol.* **2019**, *1*, 133–139.
10. Hou, Y.; Chen, D.; Yang, S. Adaptive robust trajectory tracking controller for a quadrotor UAV with uncertain environment parameters based on backstepping sliding mode method. *IEEE Trans. Autom. Sci. Eng.* **2023**; Early Access. [[CrossRef](#)]
11. Zhang, R.; Quan, Q.; Cai, K.-Y. Attitude control of a quadrotor aircraft subject to a class of time-varying disturbances. *IET Control Theory Appl.* **2011**, *5*, 1140–1146. [[CrossRef](#)]
12. Xiong, J.; Zhang, G. Global fast dynamic terminal sliding mode control for a quadrotor UAV. *ISA Trans.* **2017**, *66*, 233–240. [[CrossRef](#)]
13. Hou, Z.; Lu, P.; Tu, Z. Nonsingular terminal sliding mode control for a quadrotor UAV with a total rotor failure. *Aerosp. Sci. Technol.* **2020**, *98*, 105716. [[CrossRef](#)]
14. Alberto, I. *Nonlinear Control Systems*, 3rd ed.; Springer: London, UK, 1995.

15. Alonge, F.; D'Ippolito, F.; Fagiolini, A.; Garraffa, G.; Sferlazza, A. Trajectory robust control of autonomous quadcopters based on model decoupling and disturbance estimation. *Int. J. Adv. Robot. Syst.* **2021**, *18*, 1729881421996974. [[CrossRef](#)]
16. Zhou, D.; Jin, Z.; Wu, G. Improved Adaptive NDI Flight Control Law Design Based on Real-Time Aerodynamic Identification in Frequency Domain. *Appl. Sci.* **2023**, *13*, 6951. [[CrossRef](#)]
17. Li, Y.; Liu, X.; He, Q.; Ming, R.; Huang, W.; Zhang, W. L1 adaptive structure-based nonlinear dynamic inversion control for aircraft with center of gravity variations. *J. Intell. Robot. Syst.* **2022**, *106*, 4. [[CrossRef](#)]
18. Harris, J.; Elliott, C.M.; Tallant, G.S. L1 adaptive nonlinear dynamic inversion control for the innovative control effectors aircraft. In Proceedings of the AIAA SCITECH 2022 Forum, San Diego, CA, USA, 3–7 January 2022; p. 0791.
19. Qiao, F.; Guo, L.; Shi, J. Morphing aircraft flight control using nonlinear dynamic inversion. In Proceedings of the Advances in Guidance, Navigation and Control: Proceedings of 2020 International Conference on Guidance, Navigation and Control, ICGNC 2020, Tianjin, China, 23–25 October 2020; pp. 1519–1529.
20. Yang, H.; Cheng, L.; Xia, Y.; Yuan, Y. Active disturbance rejection attitude control for a dual closed-loop quadrotor under gust wind. *IEEE Trans. Control Syst. Technol.* **2017**, *26*, 1400–1405. [[CrossRef](#)]
21. Zhang, Y.; Chen, Z.; Zhang, X.; Sun, Q.; Sun, M. A novel control scheme for quadrotor UAV based upon active disturbance rejection control. *Aerosp. Sci. Technol.* **2018**, *79*, 601–609. [[CrossRef](#)]
22. Wang, C.; Xia, Y.; Kong, X.; Wang, T. Attitude control of underactuated quadrotor UAV based on improved ADRC. In Proceedings of the 2023 2nd Conference on Fully Actuated System Theory and Applications (CFASTA), Qingdao, China, 14–16 July 2023; pp. 699–704.
23. Lotufo, M.A.; Colangelo, L.; Perez-Montenegro, C.; Canuto, E.; Novara, C. UAV quadrotor attitude control: An ADRC-EMC combined approach. *Control Eng. Pract.* **2019**, *84*, 13–22. [[CrossRef](#)]
24. Cheng, Y.; Dai, L.; Li, A.; Yuan, Y.; Chen, Z. Active disturbance rejection generalized predictive control of a quadrotor uav via quantitative feedback theory. *IEEE Access* **2022**, *10*, 2169–3536. [[CrossRef](#)]
25. Ríos, H.; Falcón, R.; González, O.A.; Dzul, A. Continuous sliding-mode control strategies for quadrotor robust tracking: Real-time application. *IEEE Trans. Ind. Electron.* **2018**, *66*, 1264–1272. [[CrossRef](#)]
26. Jiang, T.; Zhang, F.; Lin, D. Finite-time backstepping for attitude tracking with disturbances and input constraints. *Int. J. Control Autom. Syst.* **2020**, *18*, 1487–1497. [[CrossRef](#)]
27. Zhu, W.; Wang, L.; Tian, B. Integral sliding mode control method for quadrotor unmanned aerial vehicle based on finite-time observer. *J. Chin. Inertial Technol.* **2023**, *31*, 1244–1253. [[CrossRef](#)]
28. Shtessel, Y.B.; Shkolnikov, I.A.; Levant, A.J.A. Smooth second-order sliding modes: Missile guidance application. *Automatica* **2007**, *43*, 1470–1476. [[CrossRef](#)]
29. Levant, A. Higher-order sliding modes, differentiation and output-feedback control. *Int. J. Control Autom. Syst.* **2003**, *76*, 924–941. [[CrossRef](#)]
30. Mechali, O.; Xu, L.; Senouci, A.; Xie, X.; Xin, C.; Mechali, A. Finite-time observer-based robust continuous twisting control for the attitude of an uncertain quadrotor UAV subjected to disturbances. In Proceedings of the 2020 IEEE International Conference on Mechatronics and Automation (ICMA), Beijing, China, 2–5 August 2020; pp. 1203–1208.
31. Lan, Q.; Qian, C.; Li, S. Finite-time disturbance observer design and attitude tracking control of a rigid spacecraft. *J. Dyn. Syst. Meas. Control* **2017**, *139*, 061010. [[CrossRef](#)]
32. Sun, J.; Xu, S.; Song, S.; Dong, X. Finite-time tracking control of hypersonic vehicle with input saturation. *Aerosp. Sci. Technol.* **2017**, *71*, 272–284. [[CrossRef](#)]
33. Hu, Q.; Meng, Y. Adaptive backstepping control for air-breathing hypersonic vehicle with actuator dynamics. *Aerosp. Sci. Technol.* **2017**, *67*, 412–421. [[CrossRef](#)]
34. Hu, K.-Y.; Yusuf, A.; Cheng, Z. Fuzzy adaptive backstepping control of nonlinear uncertain systems with unmeasured states and input saturation. *IEEE Access* **2020**, *8*, 228442–228453. [[CrossRef](#)]
35. Yue, Z.; Sun, J. Robust fault-tolerant control design for hypersonic vehicle with input saturation and actuator faults. *Proc. Inst. Mech. Eng. Part G J. Aerosp. Eng.* **2022**, *236*, 1563–1576. [[CrossRef](#)]
36. Kendoul, F.; Lara, D.; Fantoni, I.; Lozano, R. Real-time nonlinear embedded control for an autonomous quadrotor helicopter. *J. Guid. Control Dyn.* **2007**, *30*, 1049–1061. [[CrossRef](#)]
37. Li, S.; Wang, Y.; Tan, J. Adaptive and robust control of quadrotor aircrafts with input saturation. *Nonlinear Dyn.* **2017**, *89*, 255–265. [[CrossRef](#)]
38. Liu, K.; Wang, X.; Wang, R.; Sun, G.; Wang, X. Antisaturation finite-time attitude tracking control based observer for a quadrotor. *IEEE Trans. Circuits Syst. II Express Briefs* **2020**, *68*, 2047–2051. [[CrossRef](#)]
39. Sun, L.; Huo, W.; Jiao, Z. Disturbance-observer-based robust relative pose control for spacecraft rendezvous and proximity operations under input saturation. *IEEE Trans. Aerosp. Electron. Syst.* **2018**, *54*, 1605–1617. [[CrossRef](#)]
40. Huang, D.; Huang, T.; Qin, N.; Li, Y.; Yang, Y. Finite-time control for a UAV system based on finite-time disturbance observer. *Aerosp. Sci. Technol.* **2022**, *129*, 107825. [[CrossRef](#)]
41. Huang, X.; Lin, W.; Yang, B. Global finite-time stabilization of a class of uncertain nonlinear systems. *Automatica* **2005**, *41*, 881–888. [[CrossRef](#)]
42. Li, Y.; Yang, G. Robust fuzzy adaptive fault-tolerant control for a class of nonlinear systems with mismatched uncertainties and actuator faults. *Nonlinear Dyn.* **2015**, *81*, 395–409. [[CrossRef](#)]

43. Qian, C.; Lin, W. A continuous feedback approach to global strong stabilization of nonlinear systems. *IEEE Trans. Autom. Control* **2001**, *46*, 1061–1079. [[CrossRef](#)]
44. Hu, Q.; Jiang, B. Continuous finite-time attitude control for rigid spacecraft based on angular velocity observer. *IEEE Trans. Aerosp. Electron. Syst.* **2017**, *54*, 1082–1092. [[CrossRef](#)]
45. Bhat, S.P.; Bernstein, D.S. Finite-time stability of continuous autonomous systems. *SIAM J. Control Optim.* **2000**, *38*, 751–766. [[CrossRef](#)]
46. Zhao, Z.; Li, T.; Jiang, B.; Cao, D. Composite continuous fast nonsingular terminal sliding mode control for quadrotor UAV attitude systems. *IET Control Theory Appl.* **2023**, *40*, 459–467.

**Disclaimer/Publisher’s Note:** The statements, opinions and data contained in all publications are solely those of the individual author(s) and contributor(s) and not of MDPI and/or the editor(s). MDPI and/or the editor(s) disclaim responsibility for any injury to people or property resulting from any ideas, methods, instructions or products referred to in the content.